THE EFFECTIVENESS OF THREE-DIMENSIONAL FILM-COOLING SLOTS—II. PREDICTIONS

S. V. PATANKAR, A. K. RASTOGI and J. H. WHITELAW

Abstract—The paper reports application of the numerical procedure developed by Spalding and Patankar for three-dimensional flows, without forward recirculation, to the prediction of the effectiveness of three-dimensional film-cooling slots. The numerical procedure is based on the solution of a finite-difference representation of the time-averaged, three-dimensional boundary-layer form of the Navier–Stokes equations: thus the procedure does take account of cross-stream recirculation and is more suited to the prediction of three-dimensional film-cooling than any previous method. The numerical algorithm, which is of the forward-marching type, is unchanged from that of Spalding and Patankar but detailed changes were necessary to allow the application to the film-cooling situation: these changes are described. The turbulence model for the predictions is based on Prandtl's mixing length.

6. INTRODUCTION TO THEORETICAL INVESTIGATION

This part of the paper is concerned with the prediction of the adiabatic- or impervious-wall effectiveness downstream of three-dimensional film-cooling slots. The purposes are to present values of wall effectiveness, predicted with the aid of the three-dimensional computational method of Patankar and Spalding [4] and a simple turbulence model; to compare these predictions with the existing measurements of Part 1 and [5] and [6], and thereby to quantitatively assess the validity of the prediction procedure; and to present predicted values of effectiveness, outside the range of existing measurements, for a range of practically relevant parameters.

Previous attempts to solve differential equations appropriate to wall-jet geometries, e.g. [1, 7, 9], have been confined to two-dimensional flows although in many practical situations the slot configuration implies three-dimensional flow. This limitation arose because of the unavailability of a numerical scheme capable of solving the appropriate three-dimensional equations. The recent work of Patankar and Spalding [4] has made available a computational method for the solution of the three-dimensional, steady boundary-layer equations and provides the foundation for the work described here. Of course, the solution of any equations other than three-dimensional, unsteady Navier–Stokes equations cannot lead to an exact representation of a turbulent flow but the extension from two-dimensional procedures to a three-dimensional procedure represents a significant advance and, as will be shown, allows precise predictions which will be of assistance to designers of three-dimensional film-cooling slots.

The details of the computational method are not repeated in this paper but an outline of the salient features and the modifications which have been introduced specifically to allow the present predictions, are reported in Section 7 together with a statement of conservation equations and boundary conditions. Section 8 describes the turbulence model, indicates reasons for its selection and restates the conservation equations in the form solved. The comparisons between predicted and experimental values of effectiveness are presented in the first three sub-sections of Section 9: the last sub-section presents predicted values of effectiveness for a range of parameters of interest to designers and for which measurements are not presently available. A brief discussion of the implications

of the previous sections is contained in Section 10 and a statement of conclusions is provided in Section 11.

7. EQUATIONS AND NUMERICAL PROCEDURE

7.1 *Conservation equations and boundary conditions*

The differential equations solved by the algorithm of [4] are:

$$\frac{\partial}{\partial x}(\rho U) + \frac{\partial}{\partial y}(\rho V) + \frac{\partial}{\partial z}(\rho W) = 0 \quad (1)$$

$$\frac{\partial}{\partial x}(\rho U^2) + \frac{\partial}{\partial y}(\rho UV) + \frac{\partial}{\partial z}(\rho UW) = -\frac{\partial \bar{P}}{\partial y} + \frac{\partial}{\partial y}\tau_{u,xz} + \frac{\partial}{\partial z}\tau_{u,xy}$$

$$\frac{\partial}{\partial x}(\rho UV) + \frac{\partial}{\partial y}(\rho V^2) + \frac{\partial}{\partial z}(\rho VW) = -\frac{\partial P}{\partial y} + \frac{\partial}{\partial y}\tau_{v,xz} + \frac{\partial}{\partial z}\tau_{v,xy} \quad (2)$$

$$\frac{\partial}{\partial x}(\rho UW) + \frac{\partial}{\partial y}(\rho VW) + \frac{\partial}{\partial z}(\rho W^2) = -\frac{\partial P}{\partial z} + \frac{\partial}{\partial y}\tau_{w,xz} + \frac{\partial}{\partial z}\tau_{w,xy}$$

$$\frac{\partial}{\partial x}(\rho U\phi) + \frac{\partial}{\partial y}(\rho V\phi) + \frac{\partial}{\partial z}(\rho W\phi) = S_\phi - \frac{\partial}{\partial y}(J_{\phi,xz}) - \frac{\partial}{\partial z}(J_{\phi,xy}). \quad (3)$$

The coordinate system appropriate to the present problem is shown on Fig. 2 and the appropriate boundary conditions are:

$$U, V, W, \partial\phi/\partial y = 0 \quad \text{at } y = 0$$

$$W, \phi = 0 \quad \text{as } y \to \infty$$

$$U = U_G \quad \text{as } y \to \infty$$

$$\frac{\partial U}{\partial z}, \frac{\partial V}{\partial z}, W, \frac{\partial \phi}{\partial z} = 0 \quad \text{at } z = 0$$

$$\frac{\partial U}{\partial z}, \frac{\partial V}{\partial z}, W, \frac{\partial \phi}{\partial z} = 0 \quad \text{at } z = P_i/2$$

or

$$\phi = 0 \quad \text{as } z \to \infty$$

$$U = U_G \quad \text{as } z \to \infty.$$

Equations (1)–(3) have mean-flow properties as dependent variables and imply the need for further information about the diffusion terms: this information is provided in the form of the turbulence model discussed in Section 8. The equations contain a second approximation in that the gradients of shear stress and diffusion fluxes in the yz plane are assumed to be negligible. In more physical terms this means that the equations take account of recirculation in the planes of constant x but not in planes of constant y and z and so downstream (i.e. large values of x) properties of the flow do not influence the upstream flow. It should be noted that the term $\bar{P}$, in the U-momentum equation, is an average pressure and, for the present flow configuration its gradient in the x-direction is zero.

7.2 *Principal feature of the numerical procedure*

The presence of the longitudinal convective terms render equations (2) and (3) parabolic. The numerical procedure takes advantage of this and solves the equations by marching forward in x-direction, with the solution in the yz plane at each x-station. A suitable grid in the yz plane is chosen and initial conditions for all the dependent variables are specified. The differential equations are represented by implicit finite-difference equations which are rendered linear by calculating the coefficients using the upstream values of the variables. The difference equations are solved by employing sweeps of the tri-diagonal matrix algorithm in the y and z directions. The sequence of solving the equations is as follows. The numerical scheme assumes $\bar{P}$ to be an average pressure over a cross-section and $\partial\bar{P}/\partial x$ is taken from free stream conditions; the U-momentum equation is then solved. For the cross-stream velocity equations, P is assumed to have its upstream

value and leads to a solution which does not satisfy the continuity-equation. A correction to the assumed pressure is calculated in such a way that resulting solutions for V and W satisfy the continuity equation. After solving for the three velocity components and pressure, the equations for the other dependent variables (mass concentration, stagnation enthalpy etc.) are solved.

7.3 Special features of the numerical procedure

For the present calculations, a cross-stream grid (yz-plane) of 8×6 node points was employed for small values of t and 10×6 for large values of t. The use of this number of grid lines implies that the circular jet is represented by a shape slightly different from a circle. The mass-flow emerging from the numerical non-circular holes was ascertained to be within 2 per cent of the specified initial value and the mixing of the jets was assumed to be uninfluenced by the small deviations from roundness. A single sweep of the tridiagonal matrix algorithm in each of the y and z directions was found adequate for the calculation of U, V and W; three sweeps were necessary to ensure that the correct value of P was calculated and, thereby, continuity satisfied; five sweeps were necessary to obtain accurate solutions for ϕ. All computations were carried out on a CDC 6600 and approximately 55 s of machine time were required to obtain one of the curves of Fig. 11.

Initial profiles of the dependent variables U and ϕ at the slot exit were taken from experiment wherever available; otherwise appropriate profiles were assumed. The initial values of V and W were assumed zero. In the initial region, the non-uniformity of the U-profile resulted in oscillations and consequent divergence of the solution. This was corrected by iteration and under-relaxation of the velocity components. Gradually, with increasing downstream distance, the number of iterations was reduced and after 20 diameters no iteration was required.

For calculations of the flow downstream of a row of holes, the control volume was $P_i/2$ wide and the boundary conditions in the plane of the $P_i/2$ boundary conformed to a plane of symmetry. For single-hole calculations, the jet was allowed to spread freely in the y- and z-directions. Consequently boundary values for V and W, at the free boundary, were obtained by performing a mass balance for the forward step.

8. TURBULENCE MODEL

A consequence of the use of mean flow equations is the need to provide information of the shear stresses in terms of dependent or independent variables. In the present case an effective-viscosity hypothesis is assumed and equations (2) and (3) become:

$$\frac{\partial}{\partial x}(\rho U^2) + \frac{\partial}{\partial y}(\rho UV) + \frac{\partial}{\partial z}(\rho UW) = -\frac{\partial \bar{P}}{\partial x} + \frac{\partial}{\partial y}\left(\mu_{\text{eff}}\frac{\partial U}{\partial y}\right) + \frac{\partial}{\partial z}\left(\mu_{\text{eff}}\frac{\partial U}{\partial z}\right)$$

$$\frac{\partial}{\partial x}(\rho UV) + \frac{\partial}{\partial y}(\rho V^2) + \frac{\partial}{\partial z}(\rho VW) = -\frac{\partial P}{\partial y} + \frac{\partial}{\partial y}\left[\mu_{\text{eff}}\left(2\frac{\partial V}{\partial y}\right)\right] + \frac{\partial}{\partial z}\left[\mu_{\text{eff}}\left(\frac{\partial V}{\partial z} + \frac{\partial W}{\partial y}\right)\right] \quad (4)$$

$$\frac{\partial}{\partial x}(\rho UW) + \frac{\partial}{\partial y}(\rho VW) + \frac{\partial}{\partial z}(\rho W^2) = -\frac{\partial P}{\partial z} + \frac{\partial}{\partial y}\left[\mu_{\text{eff}}\left(\frac{\partial V}{\partial z} + \frac{\partial W}{\partial y}\right)\right] + \frac{\partial}{\partial z}\left[\mu_{\text{eff}}\left(2\frac{\partial W}{\partial z}\right)\right]$$

$$\frac{\partial}{\partial x}(\rho U\phi) + \frac{\partial}{\partial y}(\rho V\phi) + \frac{\partial}{\partial z}(\rho W\phi) = \frac{\partial}{\partial y}\left(\frac{\mu_{\text{eff}}}{\sigma_{\text{eff}}}\frac{\partial \phi}{\partial y}\right) + \frac{\partial}{\partial z}\left(\frac{\mu_{\text{eff}}}{\sigma_{\text{eff}}}\frac{\partial \phi}{\partial z}\right) \quad (5)$$

with $S_\phi = 0$ in the absence of chemical reaction. The particular form of effective viscosity used

for the present predictions is:

$$\mu_{\text{eff}} = \left\{\rho\, l^2 \sqrt{\left[\left(\frac{\partial U}{\partial y}\right)^2 + \left(\frac{\partial U}{\partial z}\right)^2\right]}\right\} + [0{\cdot}05\,(t/D)^2\,\rho_W\,\delta_W\,U_W] \qquad (6)$$

where

$$l = 0{\cdot}42y \qquad 0 < y \leqslant \frac{0{\cdot}09}{0{\cdot}42}\,y_G$$

$$l = 0{\cdot}09y_G, \qquad y > \frac{0{\cdot}09y_G}{0{\cdot}42}$$

and δ_W is defined on Fig. 2.

The numerical procedure does not, of course, require this particular assumption or even an effective-viscosity assumption. An effective viscosity assumption, based on Prandtl's mixing length, is used because experience has shown that it is the simplest turbulence model likely to provide a satisfactory degree of accuracy. The particular form used is based on the concept of separate wall-boundary layer and wake flow length scales as used for two-dimensional flows in [6]. The value of effective Prandtl number was assumed to be unity.

9. PREDICTIONS

9.1 *Comparison with multi-hole slot measurements*

The measurements contained in Part I were obtained partly to allow the testing of a prediction procedure such as that used here. Consequently they represent the most complete set of data for present purposes and have allowed the present procedure to be checked against a wide range of experiments. For reasons of space, only a sample range of comparisons are presented in this paper: the sample has been selected to indicate its range of applicability.

Figure 8 compares predictions with measurements obtained with a particular multi-hole slot and indicates the ability of the present procedure to predict the influence of velocity ratio, downstream distance and the geometrical parameter, t/D, upon the impervious-wall effectiveness. The maximum discrepancy in magnitude is 8 per cent of unity and all trends are faithfully followed.

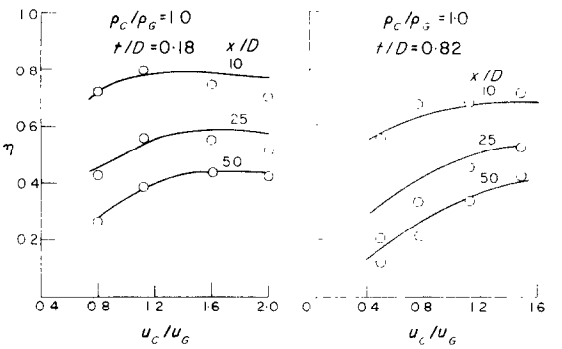

FIG. 8. Comparison between predicted values of effectiveness and measurements corresponding to Figs. 3 and 4, $\rho_C/\rho_G = 1$.

The same slot configuration was used to permit the assessment of the influence of density ratio. Measurements and predictions which demonstrate this influence are shown on Fig. 9. Again the trends are correctly predicted and the maximum difference in magnitude between measurement and prediction is 16 per cent but corresponds to a velocity ratio which is significantly smaller than those used in practice.

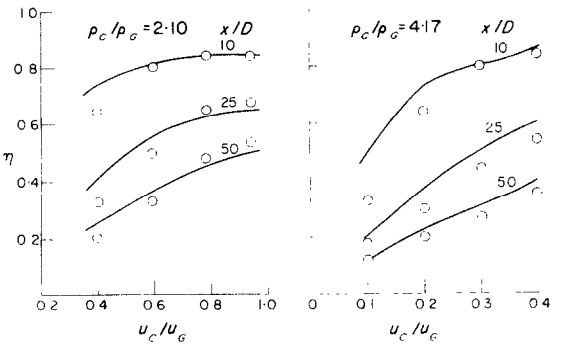

FIG. 9. Comparison between predicted values of effectiveness and measurements corresponding to Slot 1, $\rho_C/\rho_G = 2{\cdot}1$ and 4·17.

Figure 10 presents comparisons with the adiabatic-wall effectiveness measurements of

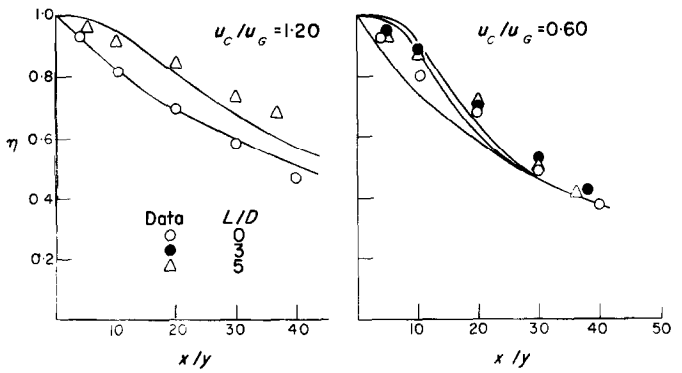

FIG. 10. Comparison between predicted values of effectiveness and the measurement of [5], $D = 10$ mm, $P_i/D = 1{\cdot}22$, $t/D = 0{\cdot}152$

[5]. Only a small sample of comparisons are presented because the uncertainties in the initial conditions assumed for the calculations may have led to significant errors. The predictions are, nevertheless in close agreement with experiment and indicate that the influence of lip

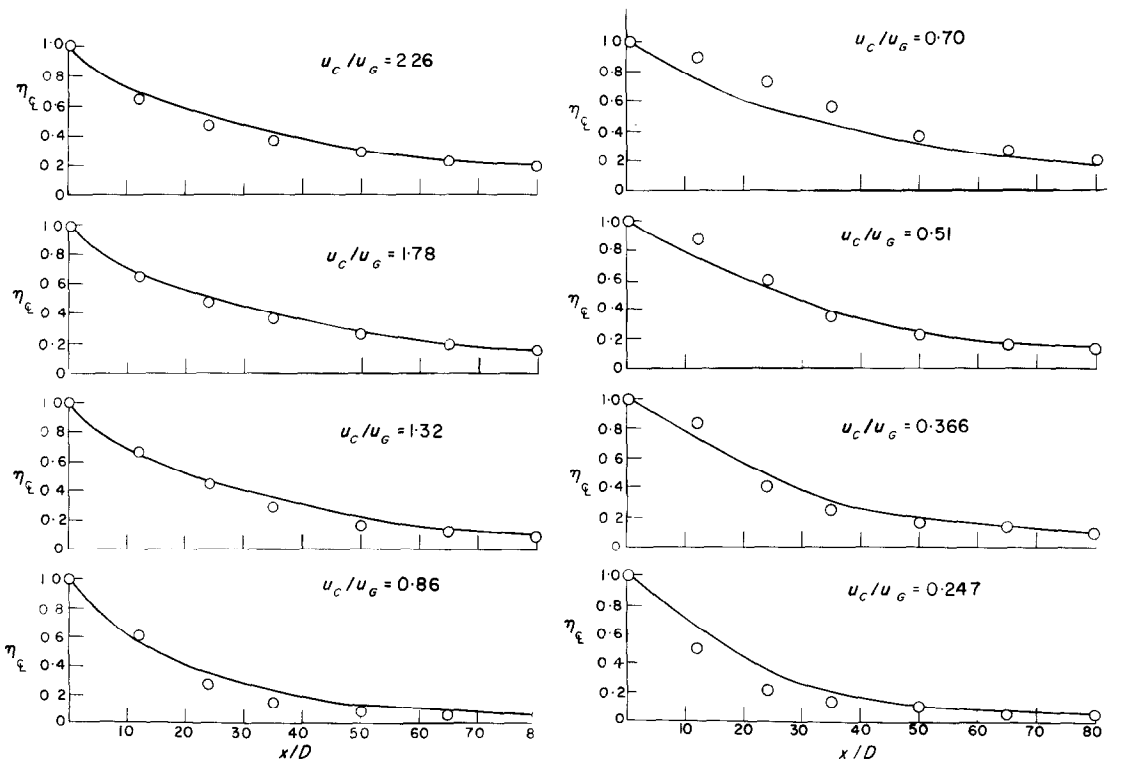

(a) $\rho_C/\rho_G = 1{\cdot}0$ (b) $\rho_C/\rho_G = 4{\cdot}17$

FIG. 11. Comparison between predicted values of effectiveness and the measurements of [6], $D = 12{\cdot}5$ mm, $t/D = 0{\cdot}18$.

length can also be predicted. The predictions with a finite lip length were achieved by applying the appropriate boundary condition at $y = y_c$ for the length of the slot lip.

9.2 *Comparison with single-hole measurements*

As indicated in Section 8.3, the assumption of a free-boundary on the z-coordinate allows predictions of effectiveness downstream of single holes. These measurements were obtained in line with the hole centre and are presented on Figs. 11a and 11b corresponding to density ratios of unity and 4·17. The constant-density results are predicted with good accuracy but the non-uniform density results are less satisfactory in the upstream region. It was expected that single-hole predictions would be less satisfactory than those for multi-hole configurations due to the greater importance of forward recirculation in the former case; this has been borne out by Fig. 11 but to a relatively small extent.

9.3 *Trends*

The comparisons presented in Sections 9.1 and 9.2 provide confidence in the ability of the prediction method to predict impervious-wall effectiveness. The procedure can now be used to predict values outside the range of available measurements and, therefore, to provide results which will guide engineers in the design of film cooling slots. Five figures are presented in this Section to indicate the dependence of impervious-wall effectiveness on practically relevant parameters for which systematic measurements are not available.

Figure 12 has been prepared to demonstrate the three-dimensionality of the impervious-wall effectiveness downstream of the multi-hole and single-hole slots for which measurements were presented earlier. Since all previous figures provide maximum values of effectiveness at any x-value, this figure allows the deviations of effectiveness, in the z direction, to be assessed. For the particular geometry of slot 1 and for the velocity ratio of 1·3, Fig. 12b suggests deviations from two dimensionality beyond 20 diameters from the slot exit.

Figures 13–16 demonstrate the influence of four geometrical parameters. The influence of the material thickness between the holes and the free-stream, t, is shown on Fig. 13 for a velocity

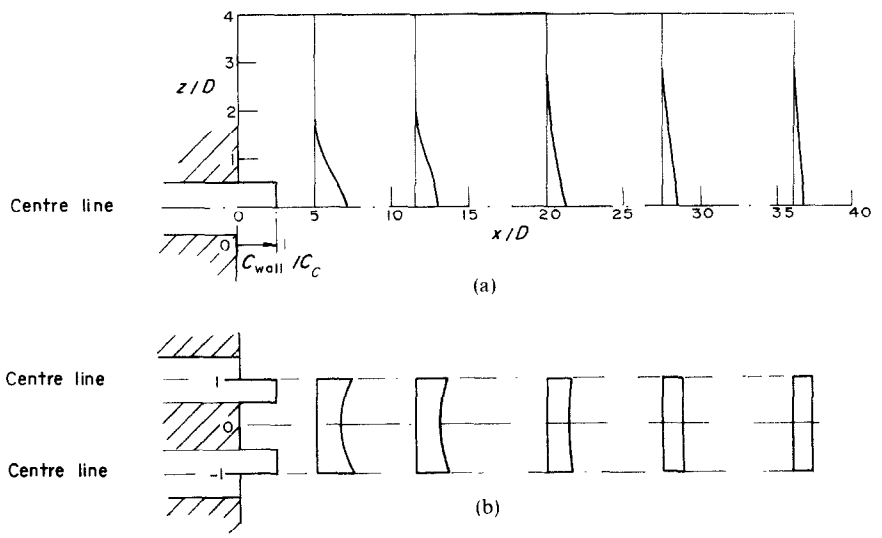

FIG. 12. Predicted variation of effectiveness in x and z directions. $U_c/U_G = 1{\cdot}3$; $\rho_c/\rho_G = 1$.

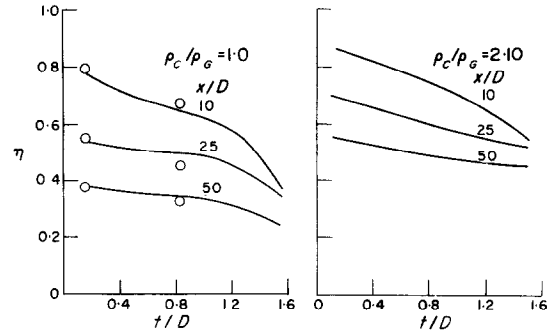

FIG. 13. Influence of t/D on effectiveness, $U_C/U_G = 1{\cdot}12$, $D = 12{\cdot}5$ mm, $P_i/D = 2$.

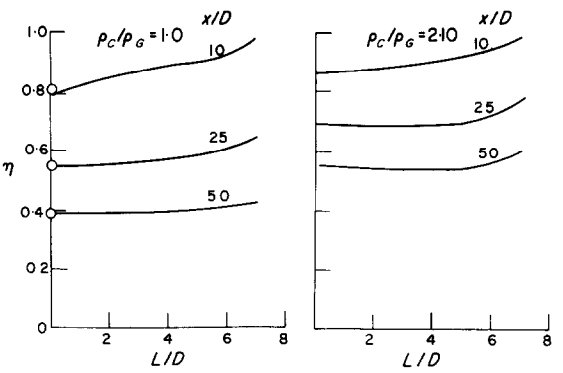

FIG. 16. Influence of L/D on effectiveness, $U_C/U_G = 1{\cdot}12$, $D = 12{\cdot}5$ mm, $P_i/D = 2$, $t/D = 0{\cdot}18$.

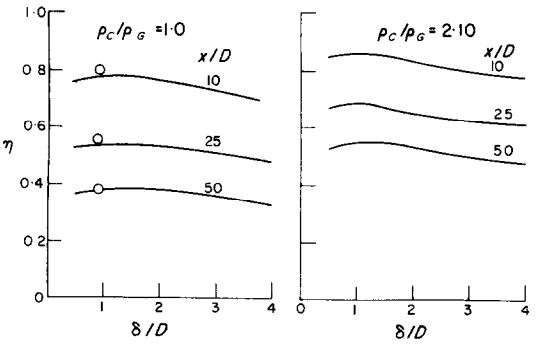

FIG. 14. Influence of δ/D on effectiveness, $U_C/U_G = 1{\cdot}12$, $D = 12{\cdot}5$ mm, $P_i/D = 2$, $t/D = 0{\cdot}18$.

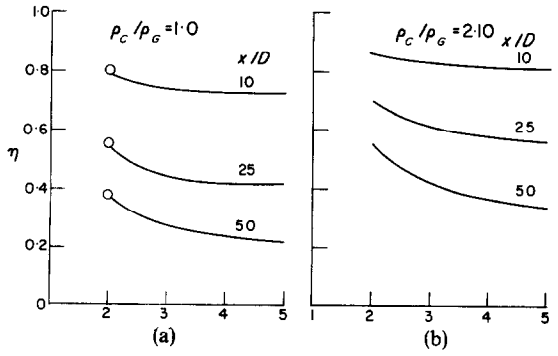

FIG. 15. Influence of P_i/D on effectiveness, $U_C/U_G = 1{\cdot}12$, $D = 12{\cdot}5$ mm, $t/D = 0{\cdot}18$.

ratio of 1·12 and for two density ratios. Measurements are shown where they exist. As was suggested by previous investigations of two-dimensional slots, an increase in t causes a decrease in η: the influence is greater for a density ratio of unity and greater for two-dimensional slots than for three-dimensional slots.

The influence of the thickness of the boundary layer on the upper surface of the slot, δ, is shown on Fig. 14 for a small value of t/D, i.e. 0·18, and for two density ratios. The influence is small but could be important in a combustion chamber where the value of δ is small at the upstream end of the chamber and, due to the build up from several films, large at the downstream end. It is the influence of δ which accounts for the difference between the measurements shown on Figs. 3 and 6.

Figure 15 is concerned with the influence of hole pitch to diameter ratio and Figs. 15a and 15b indicate this influence for uniform density and for a density ratio of 2·1 respectively. The figure shows the effect of increasing P_i/D ratio by increasing pitch for a constant mass flow rate through the slot corresponding to a velocity ratio of 1·12. It was found that the manner in which P_i/D is varied is unimportant but, of course, if P_i/D is increased by diminishing the value of D then the effectiveness at a particular x/D corresponds to a smaller x than would be in the case where P_i was increased. In practice

P_i/D should be as small as is possible with D chosen to provide a velocity ratio in the vicinity of unity.

Figure 16 demonstrates the influence of lip length with x measured from the hole exit rather than from the end of the lip. Clearly the effectiveness is improved by a finite lip and, in the practical range of L/D the influence is important close to the slot exit.

10. DISCUSSION

The results presented in Sections 9.1 and 9.2 show that the combination of the conservation equations, boundary conditions, numerical procedure and turbulence model described in Sections 7 and 8 lead to predicted values of impervious-wall effectiveness which are in good agreement with experiments. Moreover the computing times required to obtain the predictions are relatively short and support the use of the procedure for design. For combustion-chamber cooling-ring design it will, of course, only form one part of the overall energy balance which additionally requires the prediction of heat-transfer coefficient on the flame and annulus side of the cooling ring as well as the equivalent two radiation components. The procedure is presently being modified to allow the prediction of heat-transfer coefficients and measurements are in progress to test its viability.

On the basis of the experiments referred to in Part I together with [5] and [6], the various geometrical parameters have been identified and their influence understood. The present predictions quantify the influence of most of these parameters. Among the practically relevant geometrical parameters whose influence has not been predicted are the distances between the cooled surface and the edge of the holes and the presence of normal-injection holes located in line with the gaps between the tangential holes ("splash cooling"). The first of these has not been investigated because the results of [7] would suggest that, for multi-hole cooling, the influence would be small for the relatively small deviations from the tangential situation which are necessary in practice. The prediction of splash cooling will probably require consideration of the forward recirculation zone downstream of the normal jets in addition to a more sophisticated turbulence model than that employed here.

11. CONCLUSIONS

The following main conclusions may be extracted from the preceding text:

1. The numerical procedure, which solves the three-dimensional boundary-layer equations and incorporates a form of mixing-length hypothesis, predicts values of impervious-wall effectiveness which are in close agreement with experimental data. The comparisons cover a range of initial conditions which satisfactorily validate the procedure for flow and geometrical parameters similar to those found in the film-cooling of gas-turbine combustors.
2. In general terms the procedure predicts that downstream effectiveness increases with U_C/U_G, ρ_C/ρ_G, D/t, D/P_i and L/D, other parameters being constant, and quantifies these influences. The influence of each parameter and their interactions are, however, complex and the availability of the procedure greatly diminishes the need for further experiments.
3. The procedure is economical of computer time and storage, approximately 55 s and 34 K locations of CDC 6600 time and storage being required to predict the wall effectiveness for a single set of initial and boundary conditions to a downstream distance corresponding to x/D of 80.

ACKNOWLEDGEMENTS

The financial support of the Ministry of Defence, through the National Gas Turbine Establishment, is gratefully acknowledged. Discussions with NGTE personnel and with the Combustion and Systems Engineering Group of Rolls Royce (1971) Ltd., particularly M. R. Williams, have contributed significantly to the practical relevance of the work.

The authors are also grateful to Combustion Heat and Mass Transfer Ltd. for making available the basic numerical algorithm.

REFERENCES

1. B. R. Pai and J. H. Whitelaw, The prediction of wall temperature in the presence of film cooling, *Int. J. Heat Mass Transfer* **14**, 409 (1971).
2. S. C. Kacker and J. H. Whitelaw, The turbulence characteristics of two dimensional wall jets and wall wake flows, *J. Appl. Mech.* **38E**, 239 (1971).
3. A. K. Rastogi and J. H. Whitelaw, Procedure for predicting the influence of longitudinal curvature on boundary layer flows, ASME Paper No. 71-WA/FE-37.
4. S. V. Patankar and D. B. Spalding, A calculation procedure for heat, mass and momentum transfer in three dimensional parabolic flows, *Int. J. Heat Mass Transfer* **15**, 1787 (1972).
5. M. N. R. Nina and J. H. Whitelaw, The effectiveness of film cooling with three dimensional slot geometries, *J. Engng. Power* **93**, 425 (1971).
6. A. K. Rastogi and J. H. Whitelaw, Film cooling downstream of single circular tangential jets, Imperial College, Mech. Eng. Dept. Report EHT/TN/A/33 (1971).
7. L. Matthews and J. H. Whitelaw, Film cooling effectiveness in the presence of a backward facing step, Imperial College, Mech. Eng. Dept. Report EHT/TN/A/34 (1971); See also, Proceedings of the 4th All-Soviet Union Conference on Heat and Mass Transfer, Minsk (1972).
8. S. C. Kacker and J. H. Whitelaw, An experimental investigation on the influence of slot-lip thickness on the impervious wall-effectiveness of the uniform-density, two-dimensional wall jet, *Int. J. Heat Mass Transfer* **12**, 1196 (1969).
9. S. C. Kacker and J. H. Whitelaw, Prediction of wall-jet and wall-wake flows, *J. Mech. Engng Sci.* **12**, 404 (1970).

EFFICACITE DES FENTES DE REFROIDISSEMENT PAR FILM TRIDIMENSIONNEL II: ESTIMATIONS

Résumé—L'article traite de l'application de la procédure numérique développée par Spalding et Patankar pour des écoulements tridimensionnels sans recirculation ultérieure, à l'estimation de l'efficacité des fentes de refroidissement par un film tridimensionnel. La procédure numérique est basée sur la solution d'une représentation aux différences finies de l'équation de Navier-Stokes mise en forme de moyenne temporelle pour représenter une couche limite tridimensionnelle; la procédure tient compte de la recirculation transversale et elle convient au calcul du refroidissement en film tridimensionnel mieux que toute autre méthode antérieure. L'algorithme numérique, pas à pas dans le temps, est celle de Spalding et Patankar mais des changements de détail ont été apportés pour l'appliquer au cas du film réfrigérant; on décrit ces modifications. Le modèle de turbulence utilisé dans ces calculs est basé sur la longueur de mélange de Prandtl.

DIE WIRKSAMKEIT VON KÜHLSCHLITZEN FÜR DREI-DIMENSIONALE FILMKÜHLUNG—II. BERECHNUNG

Zusammenfassung—Es wird über die Anwendung des von Spalding und Patankar für drei-dimensionale Strömung ohne Vorwärts-Rezirkulation entwickelten numerischen Verfahrens auf die Berechnung der Wirksamkeit von Kühlschlitzen für die drei-dimensionale Filmkühlung berichtet. Das numerische Verfahren beruht auf der Lösung der "finiten Differenzen" der Darstellung der Navier–Stokes-Gleichungen in zeitgemittelter, drei-dimensionaler Grenzschichtform. Damit berücksichtigt das Verfahren die Querstrom-Rezirkulation und ist besser als jede andere Methode zur Berechnung der drei-dimensionalen Filmkühlung geeignet. Der numerische Algorithmus, hier in Vorwärtsschritten arbeitend, ist derselbe wie der von Spalding und Patankar. Wesentliche Änderungen waren nur erforderlich, um die Anwendung auf die Filmkühlung zu gestatten. Diese Änderungen werden beschrieben. Das Turbulenzmodell für die Berechnung basiert auf der Prandtl'schen Mischungslänge.

ЭФФЕКТИВНОСТЬ ТРЕХМЕРНЫХ ОТВЕРСТИЙ ДЛЯ ПЛЕНОЧНОГО ОХЛАЖДЕНИЯ. 2. РАСЧЕТЫ

Аннотация—Рассматривается случай применения числового метода, разработанного Сполдингом и Патанкаром для трехмерных течений без обратных циркуляционных течений для расчета эффективности трехмерных отверстий для пленочного охлаждения. Метод основан на решении усредненного во времени, трехмерного уравнения Навье-Стокса для пограничного слоя в конечно-разностном виде. Таким образом, при использовании этого метода учитывается поперечная циркуляция, и метод больше подходит для расчетов трехмерного пленочного охлаждения, чем какой-либо другой. Числовой алгоритм типа прогонки не изменяется по сравнению с алгоритмом Сполдинга и Патанкара. Но для случая пленочного охлаждения необходимы изменения, и в статье дается их описание. Турбулентная модель, используемая для расчетов, основана на длине смешения Прандтля.